Constraints on Randall-Sundrum model from the events of dijet production with QCD next-to-leading order accuracy at the LHC

Shi Ang Li,[1] Chong Sheng Li,[1,2,*] Hai Tao Li,[1] and Jun Gao[3]

[1]*Department of Physics and State Key Laboratory of Nuclear Physics and Technology, Peking University, Beijing 100871, China*

[2]*Center for High Energy Physics, Peking University, Beijing 100871, China*

[3]*Department of Physics, Southern Methodist University, Dallas, Texas 75275-0181, USA*

(Received 21 August 2014; published 23 January 2015)

We study the dijet production in the Randall–Sundrum model at the LHC with QCD next-to-leading (NLO) order accuracy. Our results show that the QCD NLO corrections can increase the total cross sections by more than 80% and reduce the scale dependence. We also explore in detail several important kinematic distributions at the NLO level. Moreover, we discuss the upper limits of the Klauza-Klein graviton excluded mass range and the allowed parameter space for the coupling constant and Klauza-Klein graviton mass, using the experiment data.

DOI: 10.1103/PhysRevD.91.014027 PACS numbers: 12.38.-t, 12.38.Bx, 12.60.-i

I. INTRODUCTION

Searching for new physics is one of the most important tasks at the LHC. In many extensions of the standard model (SM), there exist massive particles that couple to quarks or gluons, which may be observed as a narrow resonance in dijet production, such as the W', Z', excited quarks, axigluon, and Klauza-Klein (KK) graviton from extra dimensions. Therefore, the study of dijet events provides a possibility to probe new physics effects. In the SM, the dijet events are mostly produced through QCD interactions in hadron colliders, which predicts a smooth and steeply falling dijet mass spectrum. Experiments at the LHC have already used the dijet invariant mass to constrain the mass of these new resonances [1–3]. The Randall–Sundrum (RS) model [4,5] is one among various new physics models which can solve the large hierarchy problem of the weak and the Plank scale.

In the RS model, the extra dimension is assumed to be located on a S_1/Z_2 orbifold, which has two fixed points, $\phi = 0$ and $\phi = \pi$. They correspond to a high energy brane and the brane we live on, respectively. A graviton is the only particle that can propagate through the bulk between these two branes. The five-dimensional warped matric is given by

$$ds^2 = e^{-2kr|\phi|}\left(\eta_{\mu\nu} + \frac{2}{M_P^{3/2}} h_{\mu\nu}\right) dx^\mu dx^\nu - r^2 d\phi^2,$$
$$0 \le |\phi| \le \pi, \tag{1}$$

where ϕ is the five-dimensional coordinate, k is a scale of order of the Plank scale, r is the compactification radius of the extra-dimensional circle, and $h_{\mu\nu}$ is the graviton metric. Solving the five-dimensional Einstein equation and using Eq. (1), we can get the relation between the four-dimensional reduced Plank scale $\bar{M}_p$ and the five-dimensional Plank scale M_P [4],

$$\bar{M}_p = \frac{M_P^3}{k}(1 - e^{-2kr\pi}). \tag{2}$$

The physical mass m of a field in four dimensions is related to the fundamental mass parameter m_0 as the following:

$$m = e^{-kr\pi} m_0. \tag{3}$$

Thus, the hierarchy problem can be solved by assuming $kr \sim 12$.

There also exist KK towers of the massive spin-2 graviton that can interact with the SM fields, and their four-dimensional effective Lagrangian is given by [6,7]

$$\mathfrak{L} = -\frac{1}{\bar{M}_p} T^{\alpha\beta}(x) h^{(0)}_{\alpha\beta}(x) - \frac{1}{\Lambda_\pi} T^{\alpha\beta}(x) \sum_{n=1}^{\infty} h^{(n)}_{\alpha\beta}(x), \tag{4}$$

with

$$\kappa = \frac{1}{\Lambda_\pi} = \frac{1}{\bar{M}_p} e^{2kr\pi} = \frac{x_1 k}{m_{\mathrm{KK}} \bar{M}_p}, \tag{5}$$

where κ stands for the coupling constant between the KK graviton and SM particles and Λ_π is around the electroweak scale. m_{KK} is the mass of the first KK excitation mode of the graviton, which we will focus on in this paper. x_1 is the first root of the first-order Bessel function. Then the masses of the first KK excitation modes are given by

$$m_{\mathrm{KK}} = k x_1 e^{-kr\pi} = \frac{k}{\bar{M}_p} \frac{x_1}{\kappa}. \tag{6}$$

From Eqs. (5) and (6), the graviton sector of the RS model is completely determined by two parameters m_{KK} and $k/\bar{M}_p$.

*csli@pku.edu.cn

The RS KK graviton can be produced through both the gg fusion and the $q\bar{q}$ annihilation at the leading order (LO). The detailed Feynman rules of the graviton couplings can be found in Ref. [8], and the propagator for the massive spin-2 KK states is [9]

$$P^{G}_{\mu\nu,\rho\sigma}(k) = \frac{i}{2}\frac{B_{\mu\nu,\rho\sigma}(k)}{k^2 - m^2_{\rm KK} + im_{\rm KK}\Gamma_{\rm KK}}, \tag{7}$$

where

$$\begin{aligned} B_{\mu\nu,\rho\sigma}(k) = &\left(\eta_{\mu\rho} - \frac{k_\mu k_\rho}{m^2_{\rm KK}}\right)\left(\eta_{\nu\sigma} - \frac{k_\nu k_\sigma}{m^2_{\rm KK}}\right) \\ &+ \left(\eta_{\mu\sigma} - \frac{k_\mu k_\sigma}{m^2_{\rm KK}}\right)\left(\eta_{\nu\rho} - \frac{k_\nu k_\rho}{m^2_{\rm KK}}\right) \\ &- \frac{2}{n-1}\left(\eta_{\mu\nu} - \frac{k_\mu k_\nu}{m^2_{\rm KK}}\right)\left(\eta_{\rho\sigma} - \frac{k_\rho k_\sigma}{m^2_{\rm KK}}\right), \end{aligned} \tag{8}$$

where $\Gamma_{\rm KK}$ is the width of the heavy resonance, respectively.

The LO cross section and the signal for dijet production via KK graviton exchange have been calculated in the RS model in Refs. [10,11]. To put more a stringent bound on the parameters of the model at the LHC, we need the QCD next-to-leading-order (NLO) corrections to promote the theoretical accuracy. Presently, many processes are available for NLO accuracy, including single KK graviton production [9,12] and graviton decay to different final states such as Drell–Yan [13,14], diphoton [15,16], ZZ [17,18], W^+W^- [19,20], Z + missing energy [21], and $t\bar{t}$ [22]. Since K factors at the NLO level in these processes are large, it is also essential to go beyond LO for dijet final state process. In this paper, we present a QCD NLO calculation to the KK-graviton production and decay in the dijet channel at the LHC and give constraints on the relative parameters with NLO accuracy through comparing with the latest dijet event data from the CMS collaboration [3].

This paper is organized as follows. In Sec. II we show the analytic results for the LO and QCD NLO cross sections and the consistent treatment for including the QCD NLO effects of KK graviton decay width. In Sec. III we present the numerical predictions for inclusive and differential cross sections at the LHC. We simulate the signal for RS KK graviton at the LHC and update the constraints on the KK graviton mass using the recent measurement with the NLO results. Some of the lengthy analytic expressions are summarized in the Appendix.

II. ANALYTICAL RESULTS

In this section, we present the analytical results for dijet production via KK graviton exchange. The QCD NLO corrections can be factorized into two independent gauge invariant parts, i.e., a KK graviton produced at the NLO with a subsequent decay at the LO and produced at the LO with a subsequent decay at the NLO, similar to the cases of Refs. [22,23]. We neglect interference between radiation in the two stages, which are expected to be small, of order $\mathcal{O}(\alpha_s\Gamma_{\rm KK}/M_{\rm KK})$ [24–26]. This whole procedure can be illustrated as

$$\begin{aligned} |\mathcal{M}^{\rm tree}_{2\to2}|^2 &= |\mathcal{M}^{\rm tree}_{\rm pro}|^2 \otimes |\mathcal{M}^{\rm tree}_{\rm dec}|^2 \otimes |P_G|^2, \\ |\mathcal{M}^{\rm real}_{2\to3}|^2 &= \{|\mathcal{M}^{\rm tree}_{\rm pro}|^2 \otimes |\mathcal{M}^{\rm real}_{\rm dec}|^2 \\ &\quad + |\mathcal{M}^{\rm real}_{\rm pro}|^2 \otimes |\mathcal{M}^{\rm tree}_{\rm dec}|^2\} \otimes |P_G|^2, \\ \mathcal{M}^{\rm tree*}_{2\to2}\mathcal{M}^{\rm loop}_{2\to2} &= \{|\mathcal{M}^{\rm tree}_{\rm pro}|^2 \otimes (\mathcal{M}^{\rm tree*}_{\rm dec}\mathcal{M}^{\rm loop}_{\rm dec}) + |\mathcal{M}^{\rm tree}_{\rm dec}|^2 \\ &\quad \otimes (\mathcal{M}^{\rm tree*}_{\rm pro}\mathcal{M}^{\rm loop}_{\rm pro})\} \otimes |P_G|^2, \end{aligned} \tag{9}$$

where we have suppressed the possible Lorentz indices here for simplicity.

A. Leading-order results

The LO Feynman diagrams for the production and decay of the KK graviton are shown in Fig. 1. After summing over spin and color of the final state particles and averaging over spin and color of the initial states, the amplitude squares are

$$\begin{aligned} \overline{|\mathcal{M}^{\rm tree}_{q\bar{q}\to q\bar{q}}|^2} = &\frac{1}{512}\kappa^4(s^4 + 10s^3t + 42s^2t^2 \\ &+ 64st^3 + 32t^4)R(s) \end{aligned} \tag{10}$$

$$\overline{|\mathcal{M}^{\rm tree}_{gg\to q\bar{q}}|^2} = -\frac{3}{256}\kappa^4 t(s^2 + 2st + 2t^2)(s+t)R(s) \tag{11}$$

$$\overline{|\mathcal{M}^{\rm tree}_{q\bar{q}\to gg}|^2} = -\frac{1}{24}\kappa^4 t(s^2 + 2st + 2t^2)(s+t)R(s) \tag{12}$$

$$\overline{|\mathcal{M}^{\rm tree}_{gg\to gg}|^2} = \frac{1}{64}\kappa^4(s^4 + 4s^3t + 6s^2t^2 + 4st^3 + 2t^4)R(s), \tag{13}$$

where the Mandelstam variables s, t, u are defined as

$$s = (p_1 + p_2)^2, \quad t = (p_1 - p_3)^2, \quad u = (p_1 - p_4)^2. \tag{14}$$

$R(s)$ represents the LO contribution from propagator for Breit–Wigner resonance, which can be written as

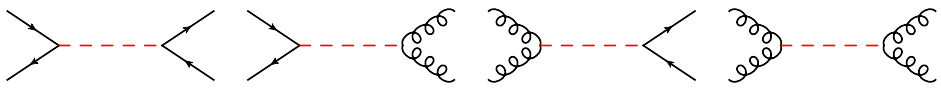

FIG. 1 (color online). Tree-level Feynman diagrams for KK graviton production and decay into dijet.

$$R(s) = \frac{1}{(s^2 - m_{\rm KK}^2)^2 + \Gamma_{\rm KK}^2 m_{\rm KK}^2}. \tag{15}$$

Throughout this paper, we work in the 't Hooft–Feynman gauge.

At hadron colliders, the LO total cross section is obtained by convoluting the partonic cross section with the parton distribution functions, which is

$$\begin{aligned}\sigma(pp \to jj) &= \sum_{q\bar{q}} \sum_{ab} \int dx_1 dx_2 [G_{q/p}(x_1,\mu_f) G_{\bar{q}/p}(x_2,\mu_f) \hat{\sigma}_{q\bar{q}\to ab} \\ &\quad + (x_1 \leftrightarrow x_2)] \\ &\quad + \sum_{ab} \int dx_1 dx_2 G_{g/p}(x_1,\mu_f) G_{g/p}(x_2,\mu_f) \hat{\sigma}_{gg\to ab},\end{aligned} \tag{16}$$

where μ_f is the factorization scale. The LO partonic cross section is defined as

$$\hat{\sigma}^B_{ij\to ab} = \frac{1}{2s} \int d{\rm PS}_2 \overline{|\mathcal{M}^{\rm LO}_{ij\to ab}|^2}. \tag{17}$$

B. NEXT-TO-LEADING-ORDER QCD CORRECTIONS

1. Virtual corrections

The loop diagrams for the production part are shown in Fig. 2. The virtual corrections contain both UV and IR divergences, with the UV divergences renormalized by introducing counterterms. Using the on-shell subtraction scheme, we define all the renormalization constants for massless quarks and gluons, which are given by

$$\begin{aligned}\delta Z_q^{\rm OS} &= -\frac{\alpha_s}{3\pi} C_\epsilon \left\{ \frac{1}{\epsilon_{\rm UV}} - \frac{1}{\epsilon_{\rm IR}} \right\}, \\ \delta Z_G^{\rm OS} &= -\frac{\alpha_S}{2\pi} \left(\frac{n_f}{3} - \frac{5}{2} \right) C_\epsilon \left\{ \frac{1}{\epsilon_{\rm UV}} - \frac{1}{\epsilon_{\rm IR}} \right\} - \frac{\alpha_S}{6\pi} C_\epsilon \left(\frac{1}{\epsilon_{\rm UV}} \right),\end{aligned} \tag{18}$$

where $C_\epsilon = \Gamma(1+\epsilon)(4\pi\mu_r^2/m_t^2)^\epsilon$ and $n_f = 5$ is the number of flavors of the massless quarks and μ_r is the renormalization scale. For the $q\bar{q}$ initial states, the renormalized virtual corrections to partonic cross section are

$$\hat{\sigma}^V_{q\bar{q}} = \hat{\sigma}^B_{q\bar{q}} \frac{\alpha_s}{2\pi} D_\epsilon \left\{ \frac{A_2^{v,q}}{\epsilon_{\rm IR}^2} + \frac{A_1^{v,q}}{\epsilon_{\rm IR}} + A_0^{v,q} \right\}, \tag{19}$$

with

$$\begin{aligned} D_\epsilon &= \frac{\Gamma(1-\epsilon)}{\Gamma(1-2\epsilon)} \left(\frac{4\pi\mu_r^2}{s} \right)^\epsilon \\ A_2^{v,q} &= -\frac{8}{3}, \\ A_1^{v,q} &= -4, \\ A_0^{v,q} &= \frac{8}{9}(\pi^2 - 15). \end{aligned} \tag{20}$$

For the gluon initial states, the renormalized virtual corrections are

$$\hat{\sigma}^V_{gg} = \hat{\sigma}^B_{gg} \frac{\alpha_s}{2\pi} D_\epsilon \left\{ \frac{A_2^{v,g}}{\epsilon_{\rm IR}^2} + \frac{A_1^{v,g}}{\epsilon_{\rm IR}} + A_0^{v,g} \right\}. \tag{21}$$

with

$$\begin{aligned} A_2^{v,g} &= -6, \\ A_1^{v,g} &= \frac{2n_f - 33}{3}, \\ A_0^{v,g} &= \frac{1}{18}(35 n_f + 36\pi^2 - 609) \\ &\quad + \frac{1}{18s} \left\{ 12 m_t^2 (6 C_0 m_t^2 + 3 C_0 s + 11) \right. \\ &\quad \left. - 12(5m_t^2 + s) \left[\ln\left(\frac{\mu_r^2}{m_t^2} \right) + \ln\left(\frac{\mu_r^2}{s^2} \right) \right] + 47 s \right\}, \end{aligned} \tag{22}$$

where C_0 is the finite scalar integral in Ref. [27], which shows as

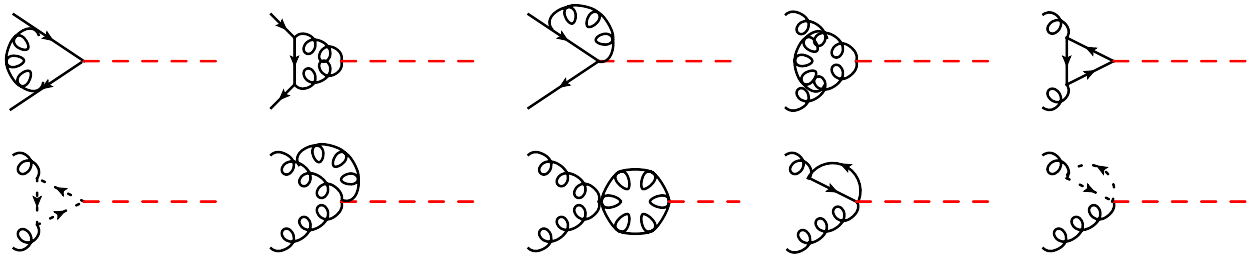

FIG. 2 (color online). One-loop Feynman diagrams for the production of the KK graviton.

$$C_0(0,0,s;m^2,m^2,m^2)$$
$$= \frac{x_s}{m^2(1-x_s^2)}\left[-\frac{1}{2}\ln^2 x_s + 2\ln(x_s)\ln(1+x_s) + 2\mathrm{Sp}(-x_s) + \frac{\pi^2}{6}\right], \quad (23)$$

with

$$\mathrm{Sp}(z) = \int_0^1 dt \frac{\ln(1-zt)}{t},$$
$$x_s = -K(s+i\epsilon, m_t, m_t),$$
$$K(z,m,m') = \frac{1-\sqrt{1-4mm'/[z-(m-m')^2]}}{1+\sqrt{1-4mm'/[z-(m-m')^2]}} \quad z \neq (m-m')^2,$$
$$K(z,m,m') = -1 \qquad z = (m-m')^2. \quad (24)$$

Note that in above renormalized amplitudes all the UV divergences cancel each other, leaving the remaining IR divergences and the finite terms.

2. Real corrections

The real corrections consist of radiation of an additional gluon, or massless quark (antiquark) in the final state. For real particle emission, the phase space integration contains both soft and collinear singularities. We adopt the two-cutoff phase space slicing method [28] to isolate all the IR singularities, where the phase space is divided into different regions by introducing two small cutoffs δ_s and δ_c. The soft cutoff δ_s separates the phase space into the soft region and hard region according to the soft condition $E_i \leq \delta_s s$, which can be written as

$$\hat{\sigma}_{ij}^R = \hat{\sigma}_{ij}^S + \hat{\sigma}_{ij}^H. \quad (25)$$

Furthermore, the hard piece is divided into two regions by collinear cutoff δ_c according to the collinear condition $-\delta_c s < (p_i - p_5)^2 < 0$,

$$\hat{\sigma}_{ij}^H = \hat{\sigma}_{ij}^{HC} + \hat{\sigma}_{ij}^{\overline{HC}}. \quad (26)$$

The $\hat{\sigma}_{ij}^{HC}$ contains the collinear divergences, which can be obtained by integration over the phase space of the emitted partons. The hard noncollinear part $\hat{\sigma}_{ij}^{\overline{HC}}$ is finite, and we can compute it using standard Monte Carlo integration techniques.

Soft gluon emission.—In the limit that the energy of the emitted gluon becomes small, i.e., $E_5 \leq \delta_s\sqrt{s}/2$, the amplitude square can be factorized into the Born amplitudes times an eikonal factor Φ_{eik},

$$\overline{\sum}|M_{\mathrm{real}}(1+2\to 3+4+5)|^2_{\mathrm{soft}} \to (4\pi\alpha_s)\sum \overline{|M_0|}^2 \Phi_{\mathrm{eik}}, \quad (27)$$

with

$$\Phi_{\mathrm{eik}} = C_I \frac{s}{p_1\cdot p_5 p_2\cdot p_5}, \quad (28)$$

where $C_I = C_F$ for the $q\bar{q}$ initial state and $C_I = C_A$ for the gg initial state. Here we only consider the situation for the initial state. Then the parton level cross section in the soft region can be expressed as

$$\hat{\sigma}_{ij}^S = \frac{1}{2s}\int \overline{|M_{\mathrm{real}}|^2}|_{\mathrm{soft}} d\Gamma_3^{\mathrm{soft}}, \quad (29)$$

where $d\Gamma_3^{\mathrm{soft}}$ is the three-body phase space in the soft region, which can be factorized:

$$d\Gamma|_3^{\mathrm{soft}} = d\Gamma_2\left[\left(\frac{4\pi}{s}\right)^\epsilon \frac{\Gamma(1-\epsilon)}{\Gamma(1-2\epsilon)}\frac{1}{2(2\pi)^2}\right]dS, \quad (30)$$

with

$$dS = \frac{1}{\pi}\left(\frac{4}{s}\right)^{-\epsilon}\int_0^{\delta_s\sqrt{s}/2} dE_5 E_5^{1-2\epsilon}\sin^{1-2\epsilon}\theta_1 d\theta_1 \sin^{-2\epsilon}\theta_2 d\theta_2. \quad (31)$$

After the integration over the soft gluon phase space, we have

$$\hat{\sigma}_{ij}^S = \frac{\alpha_s}{2\pi}\hat{\sigma}_{ij}^B D_\epsilon\left(\frac{A_2^s}{\epsilon^2} + \frac{A_1^s}{\epsilon} + A_0^s\right), \quad (32)$$

with

$$A_2^s = 2C_I,$$
$$A_1^s = -4C_I\ln\delta_s,$$
$$A_0^s = 4C_I\ln^2\delta_s. \quad (33)$$

For soft gluon radiated from outgoing partons, it gives the same results. Here we do not show their expressions.

Collinear emission.—In this section we discuss the collinear singularities in σ_{HC}, which is treated differently according to whether the singularities are from the initial or final state.

Initial state collinear radiation.—The real emission diagrams from initial states are shown in Fig. 3. In the hard collinear region, $E_5 > \delta_s\sqrt{s}/2$ and $0 < -t_{i5} < \delta_c s$, the emitted hard gluon (quark) is collinear to one of the incoming partons. As a consequence of the factorization theorem, the matrix element square can be factorized into the product of the born amplitude square and the Altarelli–Parisi splitting functions $P_{ij}(z,\epsilon)$ [29],

$$\overline{\sum}|M_3(1+2\to 3+4+5)|^2_{\mathrm{coll}} \to (4\pi\alpha_s\mu_r^{2\epsilon})\sum\overline{|M_0|}^2\left[\frac{-2P_{1'1}(z,\epsilon)}{zt_{15}} + \frac{-2P_{2'2}(z,\epsilon)}{zt_{25}}\right]. \quad (34)$$

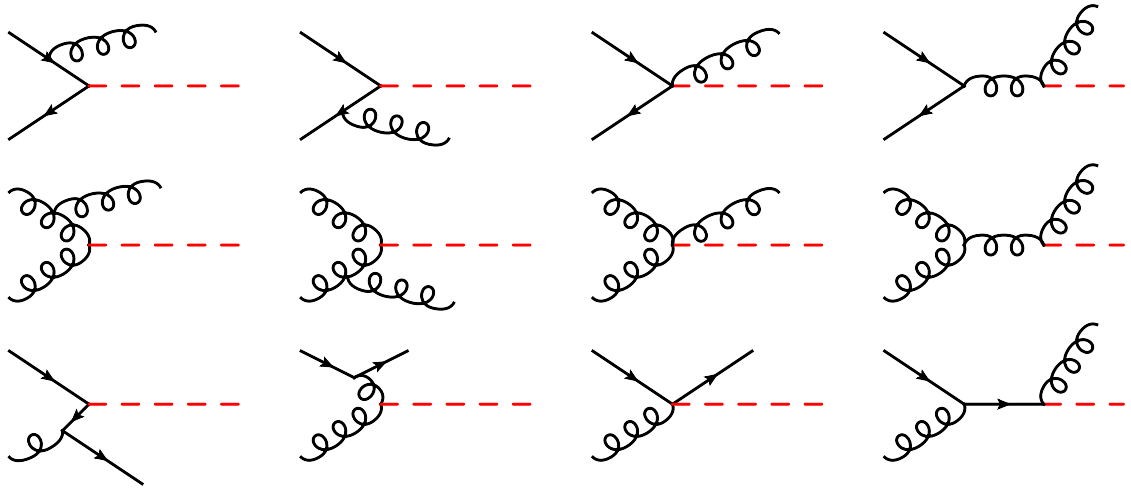

FIG. 3 (color online). Real correction Feynman diagrams for the production of the KK graviton.

Here z denotes the fraction of the momentum of 1 (2) carried by parton $1'$ ($2'$) with the emitted parton 5 taking a fraction $(1-z)$.

Moreover, the collinear three body final phase space can be factorized in the collinear limit. For example, in the limit $0 < -t_{15} < \delta_c s$, it has the following form [28]:

$$d\Gamma_3(1+2\to 3+4+5)|_{\rm coll} \to d\Gamma(1'+2\to 3+4)|_{s'=zs} \times \frac{(4\pi)^\epsilon}{16\pi^2\Gamma(1-\epsilon)} dz dt_{15}[-(1-z)t_{15}]^{-\epsilon}. \quad (35)$$

Substituting the matrix elements square and phase space in collinear limits into the hard collinear cross section, we have

$$\begin{aligned} d\sigma_{ij}^{HC} = {} & \frac{\alpha_s}{2\pi} D_\epsilon \left(-\frac{1}{\epsilon}\right) \delta_c^{-\epsilon} \{ d\hat{\sigma}^B_{q\bar{q}} [P_{1'1}(z,\epsilon) G_{1/p}(x_1/z) G_{2/p}(x_2) \\ & + P_{2'2}(z,\epsilon) G_{2/p}(x_1/z) G_{1/p}(x_2) + (x_1 \leftrightarrow x_2)] \\ & + d\hat{\sigma}^B_{gg} [P_{1'1}(z,\epsilon) G_{1/p}(x_1/z) G_{2/p}(x_2) \\ & + P_{2'2}(z,\epsilon) G_{2/p}(x_1/z) G_{1/p}(x_2)] \} \\ & \times \frac{dz}{z} \left(\frac{1-z}{z}\right)^{-\epsilon} dx_1 dx_2, \end{aligned} \quad (36)$$

where $G_{i/P}$ is the bare parton distribution function (PDFs).

Final state collinear radiation.—The real emission diagrams from final states are shown in Fig. 4. The treatment of the final state collinear singularities is much the same as that in the previous case of the initial state situation. But for indistinguishable final states, there is no need to introduce fragmentation functions. For process $1+2\to 3+4+5$ with 5 splitting from parton 4, following similar treatment as for the initial state, we have

$$d\sigma_{HC}^{1+2\to 3+4+5} = d\sigma_0^{1+2\to 3+4'} \frac{\alpha_s}{2\pi} D_\epsilon \left(-\frac{1}{\epsilon}\right) \delta_c^{-\epsilon} \times \int dz z^{-\epsilon} (1-z)^{-\epsilon} P_{44'}(z,\epsilon). \quad (37)$$

Expanding the integrand and performing the integration over z yields the final state hard-collinear terms

$$d\sigma_{HC,F}^{1+2\to 3+4+5} = d\sigma_0^{1+2\to 3+4'} \frac{\alpha_s}{2\pi} D_\epsilon \left(\frac{A_1^{4'\to 45}}{\epsilon} + A_0^{4'\to 45}\right), \quad (38)$$

where

$$\begin{aligned} A_1^{q\to qg} &= C_F(3/2 + 2\ln\delta_s), \\ A_0^{q\to qg} &= C_F[7/2 - \pi^2/3 - \ln_{\delta_s} - \ln\delta_c(3/2 + 2\ln\delta_s)], \\ A_1^{g\to q\bar{q}} &= -n_f/3, \\ A_0^{g\to q\bar{q}} &= n_f/3(\ln\delta_c - 5/3), \\ A_1^{g\to gg} &= C_A(11/6 + 2\ln\delta_s), \\ A_0^{g\to gg} &= C_A[67/18 - \pi^2/3 - \ln^2\delta_s - \ln\delta_c(11/6 + 2\ln\delta_s)]. \end{aligned} \quad (39)$$

Hard noncollinear emission.—We also have to consider contributions from the hard noncollinear part, which is finite. The hard noncollinear partonic cross section is given by

$$\hat{\sigma}_{ij}^{\overline{\rm HC}} = \frac{1}{2s} \int_{\overline{\rm HC}} \bar{\sum} |M_{ij}^3|^2 dPS_3. \quad (40)$$

We can calculate the amplitude square of these real radiation diagrams directly in four dimensions. Besides the channels we have considered in the LO diagram, there are also qg and $\bar{q}g$ initial state processes. The detail results are given in the Appendix.

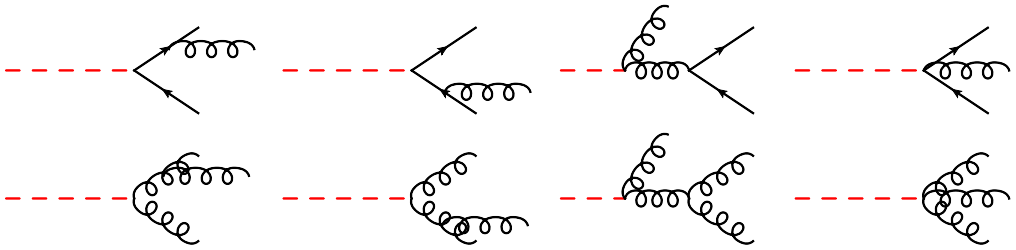

FIG. 4 (color online). Real correction Feynman diagrams for the decay of the KK graviton.

3. Mass factorization

After adding the renormalized virtual corrections and the two-cutoff real corrections, the parton level cross section still contain some collinear divergences which can be absorbed into a redefinition of the PDFs at the NLO, namely mass factorization [30]. This procedure means we replace the bare PDF $G_{a/p}(x)$ with renormalized PDF $G_{a/p}(x,\mu_f)$ and then convolute it with the partonic cross section. With the $\overline{\text{MS}}$ convention, the scale-dependent PDF $G_{a/p}(x,\mu_f)$ is given by [28]

$$G_{a/p}(x,\mu_f) = G_{a/p}(x) + \sum_b \left(\frac{1}{\epsilon}\right)\left[\frac{\alpha_s}{2\pi}\frac{\Gamma(1-\epsilon)}{\Gamma(1-2\epsilon)}\left(\frac{4\pi\mu_r^2}{\mu_f^2}\right)^{\epsilon}\right]\int_x^1 \frac{dz}{z} P_{ab}(z) G_{b/p}(x/z). \tag{41}$$

This replacement will produce a collinear singular term, which will be combined with the hard collinear contribution in Eq. (36). Then the expression for the remaining collinear contribution after considering the gg initial state contribution will be

$$\begin{aligned} d\sigma_{ij}^{\text{coll,I}} = \frac{\alpha_s}{2\pi} D_\epsilon \Bigg\{ & [\tilde{G}_{q/p}(x_1,\mu_f) G_{\bar{q}/p}(x_2,\mu_f) + G_{q/p}(x_1,\mu_f)\tilde{G}_{\bar{q}/p}(x_2,\mu_f) \\ & + \sum_{\alpha=q,\bar{q}} \left[\frac{A_1^{sc}(\alpha\to\alpha g)}{\epsilon} + A_0^{sc}(\alpha\to\alpha g)\right] G_{q/p}(x_1,\mu_f) G_{\bar{q}/p}(x_2,\mu_f) + (x_1 \leftrightarrow x_2)] d\hat{\sigma}_{q\bar{q}}^B \\ & + [\tilde{G}_{g/p}(x_1,\mu_f) G_{g/p}(x_2,\mu_f) + G_{g/p}(x_1,\mu_f)\tilde{G}_{g/p}(x_2,\mu_f) \\ & + 2\left[\frac{A_1^{sc}(g\to gg)}{\epsilon} + A_0^{sc}(g\to gg)\right] G_{g/p}(x_1,\mu_f) G_{g/p}(x_q,\mu_f)] d\hat{\sigma}_{gg}^B \Bigg\} dx_1 dx_2, \end{aligned} \tag{42}$$

where

$$\begin{aligned} A_1^{sc}(q\to qg) &= A_1^{sc}(\bar{q}\to\bar{q}g) = C_F(3/2 + 2\ln\delta_s), \\ A_1^{sc}(g\to gg) &= 2C_A\ln\delta_s + (11C_A - 2n_f)/6, \\ A_0^{sc} &= A_1^{sc}\ln\left(\frac{s}{\mu_f^2}\right), \\ \tilde{G}_{a/p}(x,\mu_f) &= \sum_{a'}\int_x^{1-\delta_s\delta_{aa'}} \frac{dy}{y} G_{a'/p}(x/y,\mu_f)\tilde{P}_{aa'}(y), \\ \tilde{P}_{ij}(y) &= P_{ij}(y)\ln\left(\delta_c\frac{1-y}{y}\frac{s}{\mu_f^2}\right) - P'_{ij}(y). \end{aligned} \tag{43}$$

Finally, the NLO total cross section for $pp\to jj$ in the $\overline{\text{MS}}$ factorization scheme is

$$\begin{aligned} \sigma^{\text{NLO}} = & \int dx_1 dx_2 [G_{q/p}(x_1,\mu_f) G_{\bar{q}/p}(x_2,\mu_f) + (x_1\leftrightarrow x_2)](\hat{\sigma}_{q\bar{q}}^B + \hat{\sigma}_{q\bar{q}}^V + \hat{\sigma}_{q\bar{q}}^S + \hat{\sigma}_{q\bar{q}}^{HC,F} + \hat{\sigma}_{q\bar{q}}^{\overline{HC}}) \\ & + \int dx_1 dx_2 G_{g/p}(x_1,\mu_f) G_{g/p}(x_2,\mu_f)(\hat{\sigma}_{gg}^B + \hat{\sigma}_{gg}^V + \hat{\sigma}_{gg}^S + \hat{\sigma}_{gg}^{HC,F} + \hat{\sigma}_{gg}^{\overline{HC}}) + \hat{\sigma}^{\text{coll,I}} \\ & + \int dx_1 dx_2 \sum_{\alpha=q,\bar{q}} [G_{g/p}(x_1,\mu_f) G_{\alpha/p}(x_2,\mu_f) + (x_1\leftrightarrow x_2)]\hat{\sigma}_{\alpha g}^{\overline{HC}}). \end{aligned} \tag{44}$$

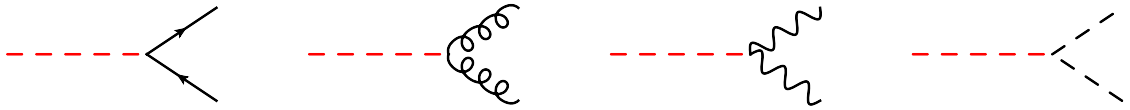

FIG. 5 (color online). Decay channels of the KK graviton.

Note that the above expression contains no singularities since $2A_2^v + A_2^s = 0$, $2A_1^{v,q} + A_1^{s,q} + 2A_1^{sc}(q \to qg) = 0$, $2A_1^{v,g} + A_1^{s,g} + 2A_1^{sc}(g \to gg) = 0$ for the initial state calculation. And similar results can be obtained for final states.

4. Consistent treatment of KK graviton decay in perturbation theory

In the narrow width approximation (NWA) [23], the production cross section for a specific decay channel is given by the total cross section times the branching fraction of the decay channel, which requires a consistent treatment of the decay at the NLO. For the Breit–Wigner resonance, there is a similar procedure. In this subsection, we briefly review the basic idea of this procedure in the NWA, then introduce the method we use for Breit–Wigner resonance.

The perturbative expansion of cross section and decay width can be written as

$$\sigma^{\mathrm{NLO}} = \sigma_0 + \alpha_s\sigma_1 \tag{45}$$

$$\Gamma^{\mathrm{NLO}} = \Gamma_0 + \alpha_s\Gamma_1. \tag{46}$$

Following the approach in Ref. [23], by expanding the cross section to $\mathcal{O}(\alpha_s)$ and discarding terms of order $\mathcal{O}(\alpha_s^2)$ or higher, we can write the differential cross sections as

$$\sigma_i^{\mathrm{NLO}} = \sigma_0 \times \frac{\Gamma_0^i}{\Gamma_0} + \sigma_0 \times \frac{\alpha_s\Gamma_1^i}{\Gamma_0} + \alpha_s\sigma_1 \times \frac{\Gamma_0^i}{\Gamma_0} - \alpha_s\sigma_0 \times \frac{\Gamma_0^i}{\Gamma_0}\frac{\Gamma_1}{\Gamma_0}, \tag{47}$$

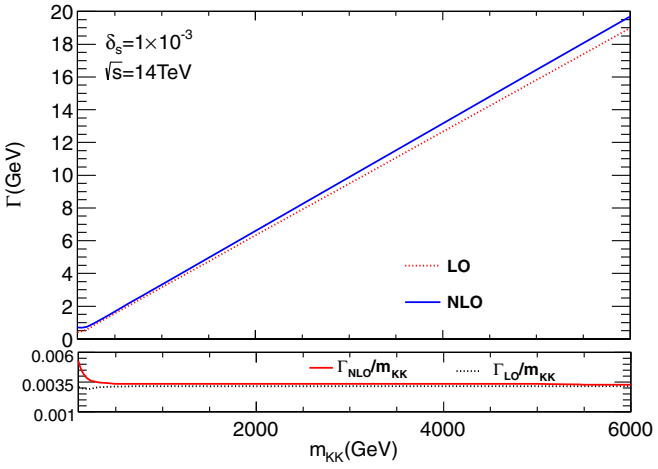

FIG. 6 (color online). The LO and NLO decay widths of the KK graviton for different KK graviton mass.

where σ_0 and Γ_0 are the lowest-order contributions to the production rate and total decay width and $\alpha_s\sigma_1$ and $\alpha_s\Gamma_1$ are the corresponding NLO corrections. Meanwhile, Γ_0^i and $\alpha_s\Gamma_1^i$ are the LO differential decay width and its NLO corrections for the channel i we considered. Following the above approach, we expand the KK graviton propagator with NLO decay width as

$$\begin{aligned}&\frac{1}{(s^2 - m_{\mathrm{KK}}^2)^2 + [\Gamma_0 + \alpha_s\Gamma_1]^2 m_{\mathrm{KK}}^2} \\ &= \frac{1}{(s^2 - m_{\mathrm{KK}}^2)^2 + \Gamma_0^2 m_{\mathrm{KK}}^2} - \frac{2\alpha_s m_{\mathrm{KK}}^2\Gamma_0\Gamma_1}{[(s^2 - m_{\mathrm{KK}}^2)^2 + \Gamma_0^2 m_{\mathrm{KK}}^2]^2}, \\ &= R(s)[1 - 2\alpha_s R(s) m_{\mathrm{KK}}^2\Gamma_0\Gamma_1],\end{aligned} \tag{48}$$

and then we can rewrite similar cross section for Breit–Wigner resonance as

$$\begin{aligned}\sigma_i^{\mathrm{NLO}} &= [1 - 2\alpha_s R(s) m_{\mathrm{KK}}^2\Gamma_0\Gamma_1]\sigma^0 \otimes \Gamma_0^i \\ &\quad + \alpha_s\sigma^1 \otimes \Gamma_0^i + \alpha_s\sigma^0 \otimes \Gamma_1^i,\end{aligned} \tag{49}$$

where in the convolution the LO width is always used in the propagator.

Now we turn to the calculations of NLO QCD corrections for the decay width of the KK graviton. The KK graviton can decay to all the particles in the SM, which is shown in Fig. 5. The LO decay width has been calculated in Ref [4], and the calculation of NLO total decay width is straight forward. Figure 6 shows the mass dependence of the LO and NLO decay width, which can be fitted as

$$\begin{aligned}\Gamma_0 &= 3.15 \times 10^{-3} m_{\mathrm{KK}}, \\ \alpha_s\Gamma_1 &= 2.08 \times 10^{-3}\alpha_s m_{\mathrm{KK}}.\end{aligned} \tag{50}$$

III. NUMERICAL RESULTS

A. Cross section

In this subsection, we present the numerical results for total and differential cross sections for dijet production via a RS KK graviton at the LHC. In our numerical calculations, we use the two-loop evaluation for $\alpha_s(Q)$ [31] and CTEQ PDFs [32]. We use the CTEQ6M PDF for the NLO calculation and CTEQ6L PDF for the LO calculation in our numerical calculations of total and differential cross sections, respectively. We assume $k/\bar{M}_p = 0.1$ and $m_{\mathrm{KK}} =$ 1.5 TeV or 2 TeV for the RS model unless specified, so the coupling strength between the graviton and the Standard

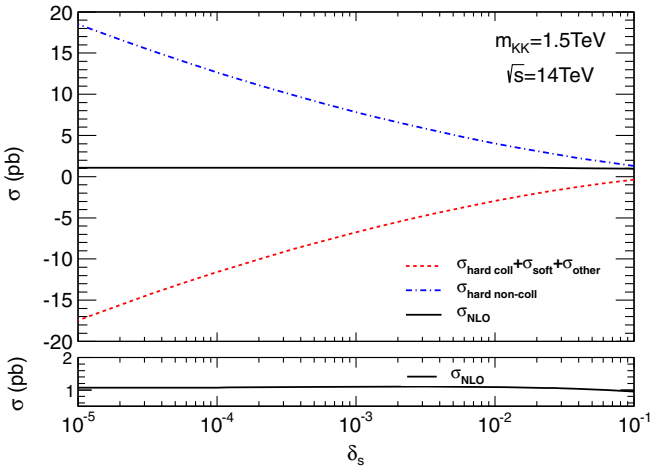

FIG. 7 (color online). Total cross sections for $pp \to G \to jj$ at the LHC as a function of δ_s in the phase space slicing treatment. The δ_c is chosen to be $\delta_c = \delta_s/50$.

Model particles will be fixed when the graviton mass is set, as shown in Eq. (5).

For the final state jets, we use the anti-k_t jet algorithm [33] with the distance parameter $D = 0.5$ to combine QCD partons into jets. We reconstruct the trigger jet using the FASTJET algorithm [34]. We also require the final state jets to satisfy the following basic kinematic cuts according to ones used in the CMS study [3],

$$p_{T_j} > 30 \text{ GeV}, \qquad |\eta_j| < 2.5.$$

Here p_{T_j} and η_j are the transverse momentum and pseudorapidity of the final state jets, respectively.

Both the renormalization and factorization scales are fixed to the invariant mass m_{jj} of the dijet final states, where $m_{jj} = \sqrt{(E_{j1} + E_{j2})^2 - |\vec{p}_{j1} + \vec{p}_{j2}|^2}$.

We have checked that the Breit–Wigner approximation is applicable at the LO and calculated the full LO results including all the channels. The results show that the contribution from the s channel, which we discuss in our work, is dominant, since contributions from the t and u channels are about 6% of the full LO total cross section. After taking the experiment kinematics requirement shown below, their contributions are extremely smaller and are only about 3%. The reason is that t and u channels are obviously suppressed by the kinematics effect from the KK graviton propagator.

In Fig. 7 we show that the dependence of the NLO total cross section on the arbitrary cutoffs δ_s and δ_c is indeed very weak. Here σ_{other} includes the contribution from the Born cross section and the virtual corrections. Both the soft plus hard collinear contributions and the hard noncollinear contributions depend strongly on the cutoffs, especially for the small cutoffs ($\delta_s < 10^{-2}$). However, after combining every contribution ($\sigma_{\text{soft}} + \sigma_{\text{hard-coll}} + \sigma_{\text{virtual}} + \sigma_{\text{hard-noncoll}}$), such dependence on the cutoffs cancels each other. The final results for σ_{NLO} are almost independent of the cutoff for $\delta_s < 10^{-2}$. We take $\delta_s = 10^{-3}$ and $\delta_c = \delta_s/50$ to obtain the numerical results presented below.

Figure 8 shows the NLO K factor, which is defined as the ratio of the NLO cross section σ_{NLO} to the LO cross section σ_{LO}, as a function of the KK graviton mass at the LHC with different center-of-mass energies. We can see that the total QCD NLO corrections can be large, which can increase the total cross sections by about 80%–100%. Numerical results show that the NLO corrections from the production part are dominant and agree with the ones given in Refs. [12,20,22]. The contributions from the decay part are relatively small but can still reach about 20%–30%.

We further present the ratios between the total cross sections from the different channels at both the LO and the NLO in Fig. 9. It can be found that the contribution from the gg channel is dominant at the low KK graviton mass region for the large PDF of the gluon, and the contribution from the $q\bar{q}$ channel becomes more important at the high mass region since the PDF of the valence quark decreases more slowly than the gluon. The NLO corrections can change the ratio between different channels significantly.

In Fig. 10, we show scale dependencies of the LO and NLO total cross sections. At the LO, the scale dependence

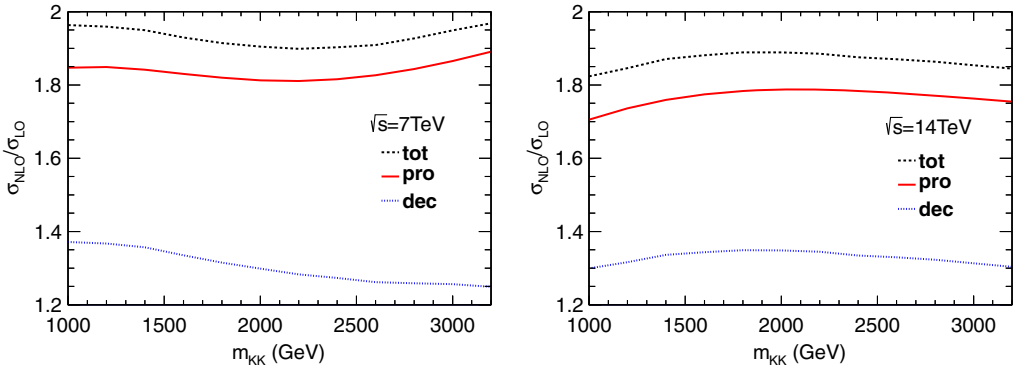

FIG. 8 (color online). The NLO K factors as functions of the heavy resonance mass at the LHC. The long dotted and solid lines correspond to including the total NLO QCD corrections and the corrections from the production part alone, respectively.

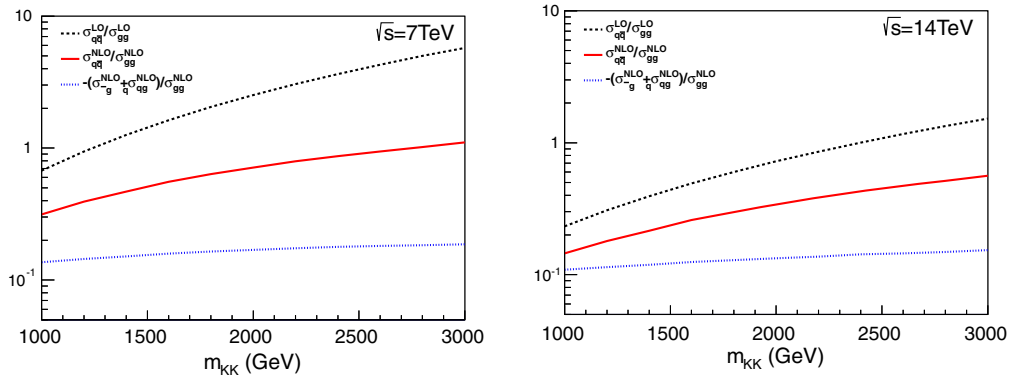

FIG. 9 (color online). The ratios of the total cross sections from different channels for the graviton as functions of the graviton mass at both the LO and the NLO.

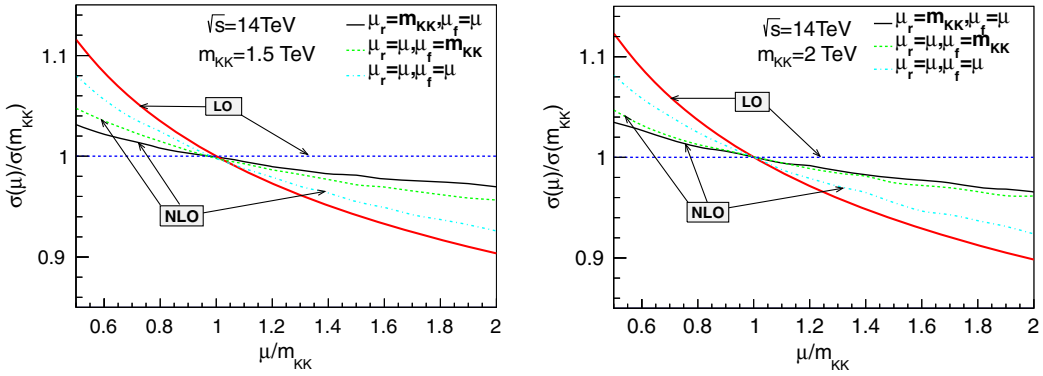

FIG. 10 (color online). Scale dependence of the total cross sections for dijet production through the RS KK graviton at the LHC with different KK graviton mass.

is purely from the factorization scale. Figure 10 shows that the factorization scale dependence of the NLO cross section is significantly reduced compared to the LO result.

B. Differential cross section

We separately present invariant mass and transverse momentum distribution in this subsection. Following the experimental analysis in Ref. [3], we consider wide jets as the final states, which are formed by clustering additional jets into the closest leading jet if within a distance $\Delta R = \sqrt{\Delta\eta^2 + \Delta\phi^2} < 1.1$. To account for resolution of the detectors, we also add a Gaussian smearing to the energy of final state jets [35], where the width is set as

$$\Delta E_j/E_j = 0.5/\sqrt{E_j/\mathrm{GeV}} \oplus 0.02. \tag{51}$$

Figure 11 gives the invariant mass distributions of the dijet. At the LO it is a Breit–Wigner distribution with a

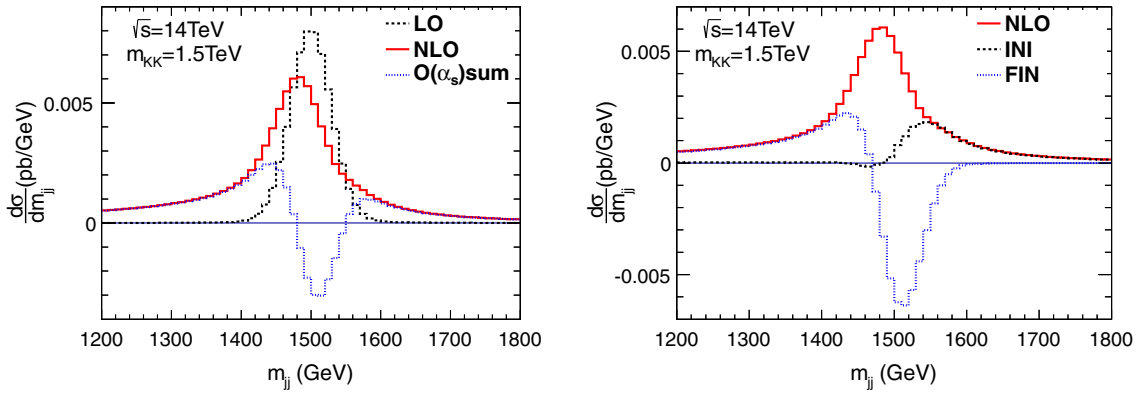

FIG. 11 (color online). Differential cross sections in the invariant mass for the final state dijet through the RS KK graviton; the left plot shows the LO, NLO results, and the NLO corrections. The right plot shows the NLO corrections from production and decay separately.

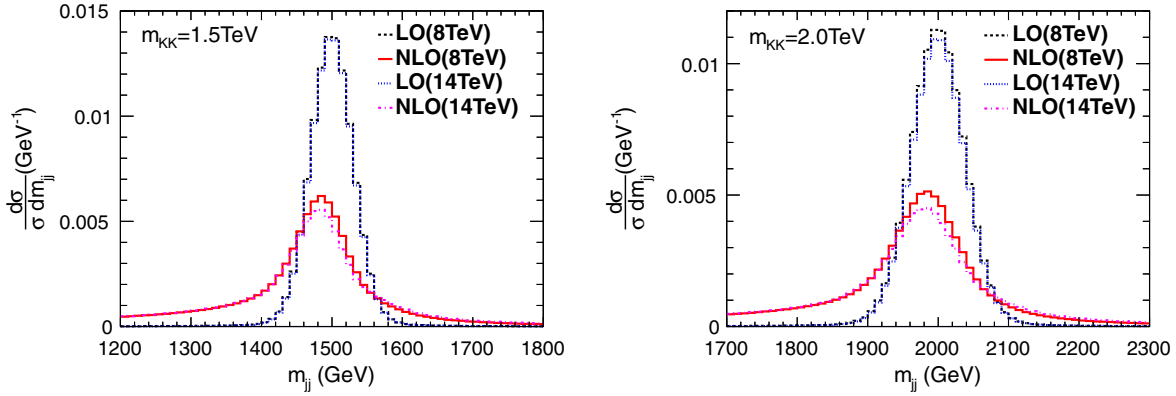

FIG. 12 (color online). Normalized differential cross sections of the invariant mass for the final state dijet through the RS KK graviton with $m_{\mathrm{KK}} = 1.5$ and 2 TeV.

center value m_{KK} and width Γ_{KK}. At the NLO there could exist an additional hard parton besides the two leading jets in the final state. Thus, the NLO corrections push the peak of the distributions to the lower invariant mass region. We also show separate contributions from initial state and final state corrections in Fig. 11. It can be seen that the initial state corrections shift the invariant mass distributions to a higher region while the final state corrections tend to shift it in the opposite way, which is a consequence of different origins of the additional radiated parton.

Figure 12 shows the normalized invariant mass distributions with different KK graviton mass and collider energy. Collider energy shows weak impact on the shape of the distribution.

In Fig. 13, we display differential cross sections for the transverse momentum p_T of the leading jet and the next-to-leading jet for different center-of-mass energies and KK graviton masses. We find that the NLO QCD corrections enhance the LO results at both low p_T and high p_T. There is a sharply falling in p_T distribution at about half the KK

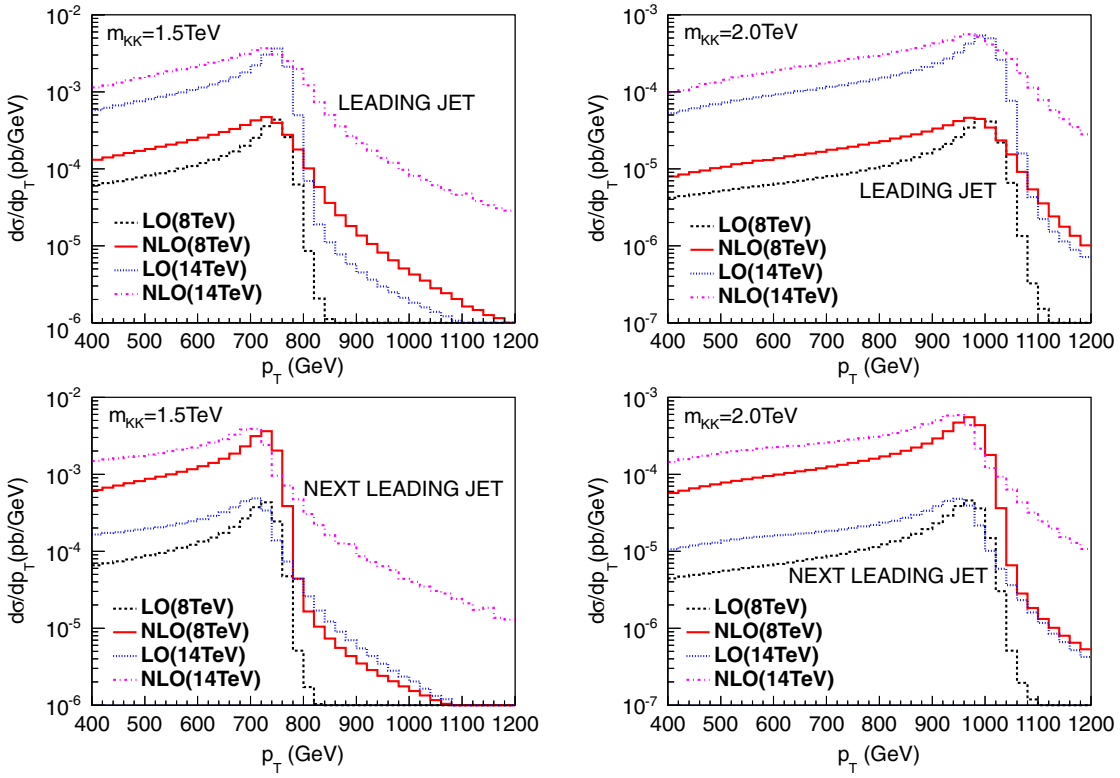

FIG. 13 (color online). The LO and NLO differential cross sections in the transverse momentum p_T of the two leading jets in dijet production. Different types of lines correspond to different collider energy. The top row shows the result for the leading jet, while the bottom row shows the result for the next-to-leading jet. The left row and right row correspond to different graviton masses.

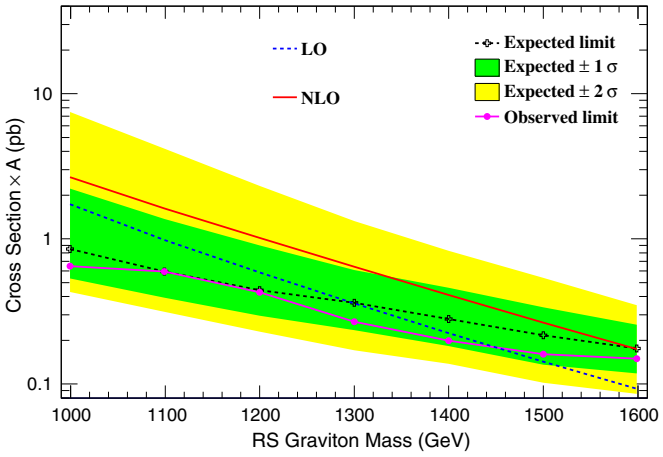

FIG. 14 (color online). Observed upper limits at 95% C.L. on $\sigma \times A$ for resonances decaying to the dijet final state compared with the expected limits and their variation at the 1σ and 2σ levels.

graviton mass, which is called the *Jacobian edge* [36]. The edge is broadened by the KK graviton width and real corrections at NLO.

C. Signal analysis

A search for the KK-graviton has been performed in the dijet mass spectrum by CMS [3], based on the LO theoretical prediction. Following Ref. [3], in Fig. 14 we present the generic upper limits at the 95% confidence level for the cross section $\sigma \times A$, where A represents efficiency due to the kinematic requirement of $|\Delta\eta_{jj}| < 1.3$ and $m_{jj} > 890$ GeV. In this subsection, we use CTEQ6M PDF for NLO calculation and CTEQ6L1 PDF for LO calculation. We also assume $k/\bar{M}_{pl} = 0.1$ for the RS model. Due to the large QCD NLO corrections, the upper limit of the excluded mass range of the graviton is promoted from 1.45 to more than 1.6 TeV.

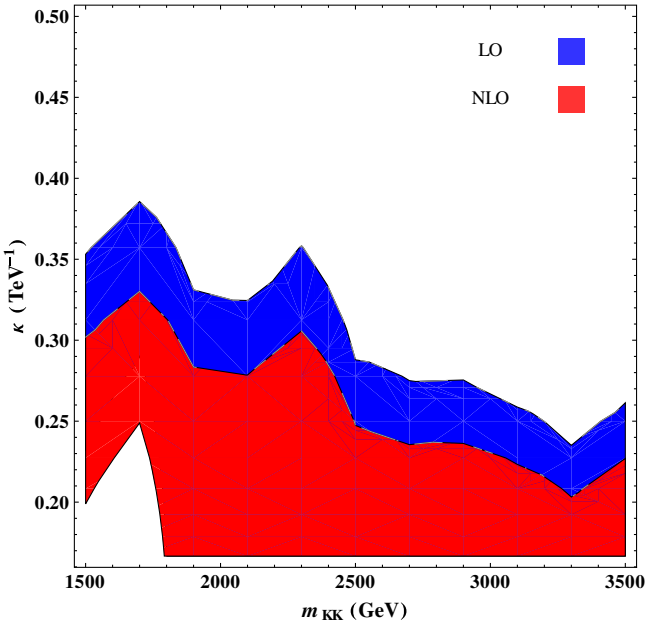

FIG. 15 (color online). Allowed parameter space (upper side, 95% C.L.) for dijet production through KK graviton at the LO and NLO.

Figure 15 shows the allowed parameter space for the KK graviton mass and its coupling to SM particles, based on the upper limit for the total cross section in Ref. [3]. In our calculation, we consider the coupling region $0.15\ \text{TeV}^{-1} \leq \kappa \leq 0.50\ \text{TeV}^{-1}$ and the mass region $1.5\ \text{TeV} \leq m_{\text{KK}} \leq 3.5\ \text{TeV}$ the same as in the experiment analysis. In Fig. 15, the red and blue region corresponds to the 95% C.L. exclusions at the LO and NLO, respectively. It can be seen from Fig. 15 that the NLO corrections significantly tighten the allowed parameter space.

IV. CONCLUSION

In conclusion, we have investigated dijet production in the RS model at the LHC, including QCD NLO corrections to the production and decay of the KK graviton. Our results show that the QCD NLO corrections increase the total cross sections by more than 80% and reduce the scale uncertainties. Furthermore, we have also explored the distributions for final state dijet invariant mass, jet transverse momentum with QCD NLO accuracy. Finally, we have discussed the constraints on the KK graviton mass and the allowed parameter space of graviton mass and its coupling, based on dijet measurement at the LHC. We have found that the upper limit of the KK graviton excluded mass range is promoted from 1.45 to more than 1.6 TeV based on our NLO calculations. The allowed parameter space is tightened as well.

ACKNOWLEDGMENTS

We would like to thank Ze Long Liu, Ding Yu Shao, and Yan Wang for helpful discussions. This work was supported in part by the National Natural Science Foundation of China under Grants No. 11375013 and No. 11135003 and by the U.S. DOE Early Career Research Award No. DE-SC0003870 and by Lightner-Sams Foundation.

APPENDIX: HARD NONCOLLINEAR PARTONIC CROSS SECTION

In this Appendix we collect the hard noncollinear amplitude square. We use Breit–Wigner approximation and ignore the interference between initial and final state radiation. For simplicity, we define the following invariant variables:

$$s_{ij} = (p_i + p_j)^2. \tag{A1}$$

For radiations from incoming partons, we have

$$\overline{|\mathcal{M}^{\text{real}}_{q\bar{q}(g)\to q\bar{q}}|^2} = -\frac{n_f\pi\alpha_s\kappa^4 s_{34}R(s)}{48(s_{13}+s_{14}-s_{34})(s_{23}+s_{24}-s_{34})(s_{13}+s_{14}+s_{23}+s_{24}-s_{34})}$$
$$\times[-3s_{34}(s_{13}^2+s_{14}^2+s_{23}^2+s_{24}^2)+3s_{34}(s_{13}+s_{14}+s_{23}+s_{s24})(s_{13}^2+s_{14}^2+s_{23}^2+s_{24}^2)$$
$$-4(s_{13}^3s_{24}+3s_{13}^2s_{14}s_{23}+3s_{13}s_{24}(s_{14}^2+s_{23}^2)+s_{14}s_{23}(s_{14}^2+s_{23}^2+3s_{24}^2))], \tag{A2}$$

and

$$\overline{|\mathcal{M}^{\text{real}}_{q\bar{q}(g)\to gg}|^2} = \frac{4\pi\alpha_s\kappa^4 s_{34}^2[s_{13}^3s_{23}+s_{13}s_{23}^3+s_{14}s_{24}(s_{14}^2+s_{24}^2)]R(s)}{9(s_{13}+s_{14}-s_{34})(s_{23}+s_{24}-s_{34})(s_{13}+s_{14}+s_{23}+s_{24}-s_{34})}, \tag{A3}$$

and

$$\overline{|\mathcal{M}^{\text{real}}_{gg(g)\to q\bar{q}}|^2} = \frac{9n_f\alpha_s\kappa^4\pi s_{34}^2R(s)}{32(s_{13}+s_{14}-s_{34})(s_{23}+s_{24}-s_{34})(s_{13}+s_{14}+s_{23}+s_{24}-s_{34})}$$
$$\times[2s_{13}^3s_{14}+2s_{13}s_{14}^3+3s_{13}^2s_{14}s_{23}+s_{14}^3s_{23}+3s_{13}s_{14}s_{23}^2+s_{14}s_{23}^3+s13^3s_{24}$$
$$+3s_{13}s_{14}^2s_{24}+3s_{13}^2s_{23}s_{24}+3s_{14}^2s_{23}s_{24}+3s_{13}s_{23}^2s_{24}+2s_{23}^3s_{24}+3s_{13}s_{14}s_{24}^2$$
$$+3s_{14}s_{23}s_{24}^2+s_{13}s_{24}^3+2s_{23}s_{24}^3-(s_{13}+s_{14}+s_{23}+s_{24})^3s_{34}+3(s_{13}+s_{14}+s_{23}+s_{24})^2s_{34}^2$$
$$-4(s_{13}+s_{14}+s_{23}+s_{24})s_{34}^3+2s_{34}^4], \tag{A4}$$

and

$$\overline{|\mathcal{M}^{\text{real}}_{gg(g)\to gg}|^2} = \frac{3\pi\alpha_s\kappa^4 s_{34}^2R(s)}{4(s_{13}+s_{14}-s_{34})(s_{23}+s_{24}-s_{34})(s_{13}+s_{14}+s_{23}+s_{24}-s_{34})}$$
$$\times\{(s_{13}^2+s_{13}s_{23}+s_{23}^2)^2-2s_{34}^3(s_{13}+s_{14}+s_{23}+s_{24})+3s_{34}^2[(s_{13}+s_{23})^2+(s_{14}+s_{24})^2]$$
$$-2s_{34}[(s_{13}+s_{23})^3+(s_{14}+s_{24})^3]+(s_{14}^2+s_{14}s_{24}+s_{24}^2)^2+s_{34}^4\}. \tag{A5}$$

The other results can be obtained by crossing symmetry.

[1] CMS Collaboration, Report No. CMS-PAS-EXO-12-016.
[2] CMS Collaboration, Report No. CMS-PAS-EXO-11-094.
[3] S. Chatrchyan *et al.* (CMS Collaboration), Phys. Rev. D **87**, 114015 (2013).
[4] L. Randall and R. Sundrum, Phys. Rev. Lett. **83**, 3370 (1999).
[5] L. Randall and R. Sundrum, Phys. Rev. Lett. **83**, 4690 (1999).
[6] J. L. Hewett, Phys. Rev. Lett. **82**, 4765 (1999).
[7] H. Davoudiasl, J. L. Hewett, and T. G. Rizzo, Phys. Rev. Lett. **84**, 2080 (2000).
[8] T. Han, J. D. Lykken, and R.-J. Zhang, Phys. Rev. D **59**, 105006 (1999).
[9] P. Mathews, V. Ravindran, and K. Sridhar, J. High Energy Phys. 10 (2005) 031.
[10] D. Atwood, S. Bar-Shalom, and A. Soni, Phys. Rev. D **62**, 056008 (2000).
[11] B. C. Allanach, K. Odagiri, M. J. Palmer, M. A. Parker, A. Sabetfakhri, and B. R. Webber, J. High Energy Phys. 12 (2002) 039.
[12] Q. Li, C. S. Li, and L. L. Yang, Phys. Rev. D **74**, 056002 (2006).
[13] P. Mathews, V. Ravindran, K. Sridhar, and W. L. van Neerven, Nucl. Phys. **B713**, 333 (2005).
[14] M. C. Kumar, P. Mathews, and V. Ravindran, Eur. Phys. J. C **49**, 599 (2007).
[15] M. C. Kumar, P. Mathews, V. Ravindran, and A. Tripathi, Nucl. Phys. **B818**, 28 (2009).
[16] M. C. Kumar, P. Mathews, V. Ravindran, and A. Tripathi, Phys. Lett. B **672**, 45 (2009).
[17] N. Agarwal, V. Ravindran, V. K. Tiwari, and A. Tripathi, Nucl. Phys. **B830**, 248 (2010).
[18] N. Agarwal, V. Ravindran, V. K. Tiwari, and A. Tripathi, Phys. Lett. B **686**, 244 (2010).
[19] N. Agarwal, V. Ravindran, V. K. Tiwari, and A. Tripathi, Phys. Rev. D **82**, 036001 (2010).
[20] N. Agarwal, V. Ravindran, V. K. Tiwari, and A. Tripathi, Phys. Lett. B **690**, 390 (2010).
[21] C. Y. Chen, H. Davoudiasl, and D. Kim, Phys. Rev. D **89**, 096007 (2014).

[22] J. Gao, C. S. Li, B. H. Li, H. X. Zhu, and C.-P. Yuan, Phys. Rev. D **82**, 014020 (2010).
[23] Q. H. Cao, R. Schwienhorst, and C.-P. Yuan, Phys. Rev. D **71**, 054023 (2005).
[24] V. S. Fadin, V. A. Khoze, and A. D. Martin, Phys. Lett. B **320**, 141 (1994).
[25] V. S. Fadin, V. A. Khoze, and A. D. Martin, Phys. Rev. D **49**, 2247 (1994).
[26] K. Melnikov and O. I. Yakovlev, Phys. Lett. B **324**, 217 (1994).
[27] W. Beenakker and A. Denner, Nucl. Phys. **B338**, 349 (1990).
[28] B. W. Harris and J. F. Owens, Phys. Rev. D **65**, 094032 (2002).
[29] G. Altarelli and G. Parisi, Nucl. Phys. **B126**, 298 (1977).
[30] G. Altarelli, R. K. Ellis, and G. Martinelli, Nucl. Phys. **B157**, 461 (1979); J. C. Collins, D. E. Soper, and G. Sterman, *Perturbative Quantum Chromodynamics*, edited by A. H. Mueller (World Scientific, Singapore, 1989).
[31] S. G. Gorishny, A. L. Kataev, S. A. Larin, and L. R. Surguladze, Mod. Phys. Lett. A **05**, 2703 (1990); Phys. Rev. D **43**, 1633 (1991); A. Djouadi, M. Spira, and P. M. Zerwas, Z. Phys. C **70**, 427 (1996); A. Djouadi, J. Kalinowski, and M. Spira, Comput. Phys. Commun. **108**, 56 (1998); M. Spira, Fortschr. Phys. **46**, 203 (1998).
[32] J. Pumplin, D. R. Stump, J. Huston, H. L. Lai, P. M. Nadolsky, and W. K. Tung, J. High Energy Phys. 07 (2002) 012.
[33] M. Cacciari, G. P. Salam, and G. Soyez, J. High Energy Phys. 04 (2008) 063.
[34] M. Cacciari, G. P. Salam, and G. Soyez, Eur. Phys. J. C **72**, 1896 (2012).
[35] G. Aad *et al.* (ATLAS Collaboration), arXiv:0901.0512.
[36] A. S. Gordon, Report No. FERMILAB-THESIS-1998-10.